Chinese Journal of Natural Medicines

Caerulomycin A disrupts glucose metabolism and triggers ER stress–induced apoptosis in triple–negative breast cancer cells

Ye Zhang, Shanshan Su, Xiaoyu Xu, Zhixian He, Yiyan Zhou, Xiangrong Lu, Aiqin Jiang

Citation: Ye Zhang, Shanshan Su, Xiaoyu Xu, Zhixian He, Yiyan Zhou, Xiangrong Lu, Aiqin Jiang, Caerulomycin A disrupts glucose metabolism and triggers ER stress–induced apoptosis in triple–negative breast cancer cells, Chinese Journal of Natural Medicines, 2025, 23(9), 1080–1091. doi: 10.1016/S1875–5364(25)60919–8.

View online: https://doi.org/10.1016/S1875–5364(25)60919–8

Related articles that may interest you

Therapeutic potential of alkaloid extract from Codonopsis Radix in alleviating hepatic lipid accumulation: insights into mitochondrial energy metabolism and endoplasmic reticulum stress regulation in NAFLD mice

Chinese Journal of Natural Medicines. 2023, 21(6), 411–422 https://doi.org/10.1016/S1875–5364(23)60403–0

Polyphyllin I promotes cell death *via* suppressing UPR–mediated CHOP ubiquitination and degradation in non–small cell lung cancer

Chinese Journal of Natural Medicines. 2021, 19(4), 255–266 https://doi.org/10.1016/S1875–5364(21)60027–4

Hernandezine promotes cancer cell apoptosis and disrupts the lysosomal acidic environment and cathepsin D maturation

Chinese Journal of Natural Medicines. 2024, 22(5), 387–401 https://doi.org/10.1016/S1875–5364(24)60638–2

Centranthera grandiflore alleviates alcohol–induced oxidative stress and cell apoptosis

Chinese Journal of Natural Medicines. 2022, 20(8), 572–579 https://doi.org/10.1016/S1875–5364(22)60181–X

Gambogenic acid induces apoptosis *via* upregulation of Noxa in oral squamous cell carcinoma

Chinese Journal of Natural Medicines. 2024, 22(7), 632–642 https://doi.org/10.1016/S1875–5364(24)60578–9

Potentilla anserina polysaccharide alleviates cadmium–induced oxidative stress and apoptosis of H9c2 cells by regulating the MG53–mediated RISK pathway

Chinese Journal of Natural Medicines. 2023, 21(4), 279–291 https://doi.org/10.1016/S1875–5364(23)60436–4

Wechat

Chinese Journal of Natural Medicines 23 (2025) 1080-1091

Contents lists available at ScienceDirect

Chinese Journal of Natural Medicines

journal homepage: www.cjnmcpu.com/

Original article

Caerulomycin A disrupts glucose metabolism and triggers ER stress-induced apoptosis in triple-negative breast cancer cells

Ye Zhang[a,Δ], Shanshan Su[a,Δ], Xiaoyu Xu[a,Δ], Zhixian He[b], Yiyan Zhou[b], Xiangrong Lu[c,*], Aiqin Jiang[a,*]

[a] *Jiangsu Key Laboratory of Molecular Medicine, Medical School of Nanjing University, Nanjing 210093, China*
[b] *Affiliated Hospital of Nantong University, Nantong 226001, China*
[c] *Nanjing University School of Life Sciences, Nanjing 210023, China*

ARTICLE INFO

Article history:
Received 3 December 2024
Revised 9 February 2025
Accepted 15 February 2025
Available online 20 October 2025

Keywords:
Triple negative breast cancer
Caerulomycin A
Glucose metabolism
CHOP
Apoptosis

ABSTRACT

Triple-negative breast cancer (TNBC) represents an aggressive breast cancer subtype with poor prognosis and limited targeted treatment options. This investigation examined the anti-cancer potential of Caerulomycin A (Cae A), a natural compound derived from marine actinomycetes, against TNBC. Cae A demonstrated selective inhibition of viability and proliferation in TNBC cell lines, including 4T1, MDA-MB-231, and MDA-MB-468, through apoptosis induction. Mechanistic analyses revealed that the compound induced sustained endoplasmic reticulum (ER) stress and subsequent upregulation of C/EBP homologous protein (CHOP) expression, resulting in mitochondrial damage-mediated apoptosis. Inhibition of ER stress or CHOP expression knockdown reversed mitochondrial damage and apoptosis, highlighting the essential role of ER stress and CHOP in Cae A's anti-tumor mechanism. Both oxygen consumption rate (OCR) and extracellular acidification rate (ECAR) decreased in TNBC cells following Cae A treatment, indicating reduced mitochondrial respiratory and glycolytic capacities. This diminished energy metabolism potentially triggers ER stress and subsequent apoptosis. Furthermore, Cae A exhibited significant anti-tumor effects in the 4T1 tumor model *in vivo* without apparent toxicity. The compound also effectively inhibited human TNBC organoid growth. These results indicate that Cae A may serve as a potential therapeutic agent for TNBC, with its efficacy likely mediated through the disruption of glucose metabolism and the induction of ER stress-associated apoptosis.

1. Introduction

Breast cancer remains the most commonly diagnosed cancer and the primary cause of cancer-related deaths among women [1]. Triple-negative breast cancer (TNBC) represents the most challenging breast cancer subtype, characterized by the highest recurrence and mortality rates [2]. Recent developments have introduced multiple targeted therapeutic approaches based on specific molecules and signaling pathways for TNBC treatment, including PI3K/AKT/mTOR inhibitors, epidermal growth factor receptor inhibitors, Notch inhibitors, poly ADP-ribose polymerase inhibitors, and antibody-drug conjugates [3-5]. Additionally, immune checkpoint inhibitors such as pembrolizumab, atezolizumab, and durvalumab are extensively studied in clinical settings [6]. Despite these therapeutic advances providing multiple treatment options for TNBC patients, they fail to address the needs of all patients. Moreover, most of these treatments remain in clinical trials, requiring further evaluation of their efficacy and safety. Consequently, investigating the anti-cancer effects and mechanisms of natural product active ingredients against TNBC presents significant potential for discovering clinically effective therapeutic drugs.

The endoplasmic reticulum (ER) serves as a crucial organelle responsible for the synthesis, folding, and modification of secreted and transmembrane proteins [7]. Disruption of ER function by various external factors and cell-intrinsic events results in unfolded protein accumulation, triggering unfolded protein response (UPR) and ER stress [8-10]. Under normal conditions, the UPR mitigates stress response and restores ER homeostasis to promote cell survival. However, during severe and irreparable ER stress, the UPR transitions from a pro-survival mode to a pro-death response through mitochondrial engagement, activating the intrinsic apoptosis pathway [11, 12]. During this process, the transcription factor ATF4 binds to the promoter region and elevates C/EBP homologous protein (CHOP) expression. CHOP, a common target gene downstream of all three apical ER sensors, initiates cell death through activation of protein synthesis-related genes [13, 14]. Furthermore, CHOP regulates Bcl-2 family protein expression, increases mitochondrial membrane permeability, and promotes cytochrome C release to form apoptotic bodies, thereby participating in the intracellular apoptotic pathway [14]. While ER stress induction represents an attractive anti-tumor therapy strategy, no ER stress-inducing anti-tumor drugs have

* Corresponding author.
E-mail addresses: 231505022@smail.nju.edu.cn(X. Lu); jianaq@nju.edu.cn (A. Jiang)
Δ These authors contributed equally to this work.

https://doi.org/10.1016/S1875-5364(25)60919-8
Copyright © 2025, China Pharmaceutical University. Published by Elsevier B.V. All rights reserved.

yet received approval for TNBC treatment.

Metabolic reprogramming of cancer cells represents a crucial strategy enabling tumor cells to adapt to rapid proliferation, invasion, metastasis, and immune escape. Tumor cells depend on elevated glucose metabolism to generate substantial ATP quantities, supporting their survival, proliferation, and resistance to apoptosis. Notably, glucose metabolism disorders can trigger ER stress by affecting ER function, subsequently regulating cell survival and death [15]. For instance, Wang [16] demonstrated that oxygen-glucose deprivation (OGD) induced up-regulation of ER stress-related proteins in human neuroblastoma SH-SY5Y cells, contributing to cell death regulation. Consequently, inducing ER stress through glucose metabolism interference has emerged as a potential cancer treatment strategy [17, 18]. Thus, promoting cancer cell apoptosis by inducing ER stress through glucose metabolism regulation presents a novel therapeutic approach. However, research in this domain remains nascent, necessitating further investigation into specific molecular mechanisms and clinical application potential.

Natural products have consistently served as a valuable source for anti-cancer drug discovery [19]. Caerulomycin A (Cae A), a natural product extracted from marine blue-green actinomycetes, features a core structure of 2,2'-bipyridine [20]. 2,2'-Bipyridine functions as a bidentate chelating ligand, forming complexes with various metal ions and exhibiting strong redox activity. Evidence indicates that iron chelators such as di-2-pyrone 4,4-dimethyl-3-semicarbazone (Dp44mT) and deferoxamine (DFO) typically induce ER stress in cancer cells [13, 21, 22]. Consequently, these oxidative active metal complexes have emerged as promising candidates for ER stress induction. Although the antibiotic and immunomodulatory properties of Cae A have been well documented, its anti-tumor activity remains poorly characterized, and its underlying mechanisms are not well understood. In this study, we demonstrated that Cae A significantly decreased cell viability and inhibited the proliferation of TNBC cells. We examined three ER stress pathways, their downstream target protein CHOP, endogenous apoptosis, and glucose metabolism imbalance. The relationships among these phenomena were investigated to elucidate Cae A's mechanism of action on TNBC. This research offers a novel perspective for TNBC treatment.

In this study, we discovered that Cae A specifically inhibited TNBC cell viability and proliferation. Cae A induced abnormal glucose metabolism in TNBC cells, effectively triggering sustained ER stress and CHOP expression, which led to mitochondrial damage-mediated apoptosis. Furthermore, Cae A demonstrated promising therapeutic effects *in vivo* in tumor-bearing mice without significant side effects. This research presents new opportunities for developing Cae A as a TNBC treatment and provides a theoretical foundation for therapeutic strategies targeting abnormal glucose metabolism and ER stress.

2. Materials and Methods

2.1. Reagents and antibodies

The following reagents were purchased from MedChemExpress: Cae A (HY-114495), 4-Phenylbutyric acid (HY-A0281), Z-VAD-FMK (HY-16658B). We would like to express our gratitude to Prof. Huimin Ge of the School of Life Sciences at Nanjing University for kindly donating part of Cae A. Primary antibodies for Western blotting were used: ATF4 (Proteintech, 10835-1-AP), ATF6 (Proteintech, 24169-1-AP), XBP1S (Proteintech, 24868-1-AP), β-Actin (Proteintech, 66009-1-Ig), Phospho-EIF2S1 (Proteintech, 28740-1-AP), Caspase-8 (Proteintech, 13423-1-AP), GAPDH (Immunoway, YM3029), IRE Phospho-thr973 (Immunoway, YP1798), PERK Phospho-thr981 (Immunoway, YP1005). The following primary antibodies were purchased from Cell Signaling Technology: B-cell lymphoma-2 (Bcl-2) (3498), Bcl-2-associated X protein (Bax) (2772), Bcl-xL (2764), BiP (3177), Cleaved-Caspase-3 (9661), Caspase-9 (9508), Cytochrome C (4272), CHOP (2895), Phospho-Histone H2A.X (9718), PARP (9532), Cleaved-PARP (9541). The goat anti-mouse secondary antibody for Western blotting was obtained from Immunoway (RS001) and goat anti-rabbit secondary antibody from Beyotime (A0208).

2.2. Cell culture

All cells were obtained from the Cell Bank, Chinese Academy of Sciences. MDA-MB-231 and MDA-MB-468 cells were maintained in Leibovitz's L-15 (BasalMedia, L620KJ) supplemented with 10% fetal bovine serum (MULTICELL, 086550013) and 1% Penicillin-Streptomycin Solution (Gibco, 15140-122) in a humidified chamber at 37 °C without CO_2. The remaining cell lines were maintained in high-glucose Dulbecco's modified Eagle medium (DMEM; VivaCell, C3113-0500) supplemented with 10% fetal bovine serum and 1% penicillin-streptomycin Solution in a humidified chamber at 37 °C under 5% (V∶V) CO_2 atmosphere.

2.3. Reverse transcription and quantitative polymerase chain reaction (qPCR)

Total ribonucleic acid (RNA) was extracted using Lysis Buffer for RNAeasy™ Animal RNA Isolation Kit (Beyotime, R0027), and 1 μg of total RNA was reverse transcribed to complementary deoxyribonucleic acid (cDNA) using a HiScript® II Q RT SuperMix (Vazyme, R222-01). ChamQ Universal SYBR qPCR Master Mix (Vazyme, Q711-02) and a QuantStudio™ 1 Real-time PCR Instrument (Thermo Fisher Scientific) were utilized to perform qPCR. The relative expression levels were calculated using the $2^{-\Delta\Delta CT}$ method. The primer sequences used for qPCR are listed in Table S1.

2.4. Western blotting

The cells treated with Cae A were placed on ice and homogenized in ice-cold radioimmunoprecipitation assay (RIPA; Beyotime, P0013B) buffer containing protease inhibitor (Invitrogen, A32961), and subsequently centrifuged at 12 000 r·min^{-1} for 20 min at 4 °C. Protein concentration was determined using the BCA method. 30 μg of protein were separated by SDS-PAGE and transferred to PVDF membranes (Bio-Rad, 1620177, USA). Following blocking with 5% skim milk, membranes were incubated overnight with primary antibodies (1∶1000). Membranes were then probed with secondary antibody (1∶2000). Signals were detected by enhanced chemiluminescence, and band intensity was quantified using ImageJ.

2.5. Cell proliferation assay

A WST-8 cell counting kit-8 (CCK-8; Dojindo, CK04) was used to evaluate the effects of Cae A on cell growth. Cells were seeded in 96-well plates at a density of 8000 cells per well and treated for 48 h. Subsequently, cells were incubated with 10 μL CCK-8 reagent for 1–2 h at 37 °C. The absorbance was measured at 450 nm using BioTek Synergy HTX (multi-mode reader).

2.6. Cell clone formation assay

Cells were seeded at a density of 1 × 10^3 cells per well and incubated with various concentrations of Cae A in six-well plates for 48 h. The medium containing 2% FBS was changed every 3 days until visible cell colonies appeared after approximately two weeks. Cells were fixed with 10% formaldehyde for 10 min and

stained with 0.1% crystal violet for 30 min. Following gentle washing with phosphate-buffered saline (PBS), cells were air-dried, photographed, and documented. Cell clones were analyzed using ImageJ software.

2.7. Transcriptome analysis

Cells were inoculated into 6-well plates and incubated with 1 μmol·L^{-1}. Cae A-treated 4T1 cells for 12 h. Cells were harvested by centrifugation, washed, and lysed with 1 mL VeZol (Vazyme, R411-01-AA) and PBS, and total RNA was isolated from the cells. Differentially expressed genes were identified through RNA-seq analysis. Relevant biological pathways and processes were analyzed using Kyoto Encyclopedia of Genes and Genomes (KEGG) pathway enrichment analysis and Gene Set Enrichment Analysis (GSEA).

2.8. Annexin V-fluorescein isothiocyanate (FITC) apoptosis assay

The apoptosis-inducing effect of Cae A was evaluated using an Annexin V-FITC/propidium iodide (PI) apoptosis detection kit (FCMCS, FMSAV-100). Cells were seeded in 6-well plates at a density of 3 × 10^5 cells per well and treated with Cae A for 48 h. Subsequently, cells were washed twice with PBS, harvested by centrifugation, and resuspended in 115 μL buffer containing 5 μL FITC Annexin V and 10 μL PI. The cells were stained for 15 min at 37 °C in the dark. Flow cytometric analysis was performed on a flow cytometer (Accuri C6; BD Bioscience, USA), analyzing at least 10 000 live cells. Data analysis was conducted using FlowJo-V10 software.

2.9. Mitochondrial membrane potential assay

Detection of Mitochondrial Membrane Potential: cells were seeded in 6-well plates (3 × 10^5 cells per well) and treated with 1 μmol·L^{-1} Cae A for 24 h according to the protocol. The cells were then incubated with 1 × JC-1 probe (Solarbio, M8650) for 20 min at 37 °C and observed using a fluorescent inverted microscope (Nikon, Japan).

2.10. Transmission electron microscopy

4T1 and MDA-MB-231 cells were treated with 1 or 4 μmol·L^{-1} Cae A for varying durations, then digested and collected. Following a single PBS wash, cells were fixed overnight at 4 °C in electron microscope fixative. The cells were subsequently washed three times with 0.1 mol·L^{-1} PB (pH 7.4) and embedded in 1% agarose. Samples were then fixed in 1% osmium tetroxide in 0.1 mol·L^{-1} PB (pH 7.4) for 2 h in the dark, followed by three buffer washes. Tissue dehydration was performed using a graded ethanol series (30% to 100%), followed by two 15-minute incubations in 100% acetone. For embedding, samples were placed in molds with pure 812 resin (Servicebio, 90529-77-4), incubated at 37 °C overnight, and polymerized at 60 °C for 48 h. Ultrathin sections were prepared and stained with 2% uranyl acetate in saturated alcohol for 8 minutes in the dark, followed by 2.6% lead citrate solution staining for 8 minutes away from CO_2. Sections were washed with ultrapure water, dried overnight at room temperature in a copper mesh box, and analyzed using a transmission electron microscope.

2.11. Immunofluorescence

For immunofluorescence imaging, cells were fixed in cold 3.7% formaldehyde solution for 15 min, rinsed, and stained with Tubulin Tracker Green (Beyotime, C1051S) for 1 h at room temperature in the dark. Following primary antibody incubation, cells were washed and counterstained with DAPI (FCMCS, FMS-FZ011-050) for 5 min at room temperature in the dark. Images were acquired using a Confocal Laser Scanning Microscope (FV3000; Olympus, Japan).

2.12. Metabolic analysis

The oxygen consumption rate (OCR) and extracellular acidification rate (ECAR) were measured through extracellular flux analysis using a Seahorse XFe96 analyser (Agilent). Cells were initially inoculated into XFe cell culture microtiter plates at a density of 8 × 10^3–1 × 10^4 and incubated at 37 °C until adherence. The cells were then treated with 4 μmol·L^{-1} Cae A for a specified period, after which pyruvate, glutamine, and glucose (pH 7.4) were added, or glucose, 2-deoxyglucose, and antimycin A/fisetinone were administered at designated time points. OCR and ECAR measurements were conducted using the Seahorse XF cellular mitochondrial stress test kit (Agilent, 103015-100) and Seahorse XF glycolysis rate assay kit (Agilent, 103020-100), respectively, following the manufacturer's protocols. Data collection was performed using Seahorse XFp Wave software, followed by analysis.

2.13. Tumor xenograft model

Six-week-old female Balb/c mice were obtained from GemPharmatech Co., Ltd. The animal study received approval from the Institutional Animal Care and Use Committee of Nanjing University. 1 × 10^5 4T1 cells suspended in 100 μL PBS were subcutaneously implanted into mice. When tumor volumes reached approximately 100 mm^3, mice were randomly assigned to three groups receiving intratumoral injections of 100 μL of Cae A (10mg·kg^{-1}·d^{-1}) or vehicle (5% Tween-80, 10% DMSO, 40% PEG400, 45% physiological saline) or nothing (negative control) (n = 5/group). Primary tumor volume measurements occurred every other day throughout the experiment using a vernier caliper, calculated as (length × width^2)/2. After approximately 3 weeks post-tumor injection, mice underwent euthanasia, and tumors were surgically excised for comparison.

2.14. Culture and treatment of organoids

Organoids were extracted from the tumor tissues of a patient with TNBC who underwent left breast malignancy resection in August 2024. The surgical samples were utilized for experimentation following informed consent and approval from the Ethics Committee of Nantong University Affiliated Hospital (2022-L126). Fresh tumor tissues underwent 3–5 rinses with PBS to eliminate mucus and debris. The tumor tissues were minced and digested using a breast cancer organoid construction kit (JIYAN, OCK-013). The resulting cell suspension was combined with pre-cooled Matrigel and seeded at 45 μL per well in a 24-well culture plate, with 0.5 mL of breast cancer organoid complete medium added to each well. The plate was maintained at 37 °C in a 5% CO_2 environment, with medium replacement every 2–3 days to ensure sufficient nutrients for organoid growth. Organoids underwent passage according to the manufacturer's instructions upon reaching 100 μm in size.

Mature organoids were harvested using organoid recovery solution and enzymatically digested into single-cell suspensions. Following cell counting, 2 × 10^3 cells per well were seeded with four replicates per concentration. The cells mixed with Matrigel were placed in a 96-well plate, with 100 μL of complete medium per well. After organoid sphere formation, Cae A was administered at concentrations of 64, 16, 4, 1, 0.25, and 0.0625 μmol·L^{-1} for 6 days. An additional complete medium containing Cae A was supplemented on day three to minimize medium evap-

oration effects. Organoid morphology was observed and documented on day six.

2.15. Statistical analysis

All data were derived from at least three independent experiments and presented as mean ± standard deviation (mean ± SD). Statistical analysis and graphing were primarily conducted using Prism 8.0.2 software. Statistical differences were determined through Student's *t*-test or analysis of variance (ANOVA). $P < 0.05$ indicated statistical significance.

3. Results

3.1. Cae A selectively inhibited the proliferation and migration of TNBC cells

To examine the potential anti-cancer effects of Cae A in tumors, various cancer cell lines, including 4T1, MDA-MB-231, MDA-MB-468 (TNBC), MCF-7 (breast cancer), Hela (cervical cancer), PANC-1 (pancreatic cancer), A549 (non-small cell lung cancer), HUH-7 (hepatoma), and HCT116 (colorectal cancer) received treatment with gradient doses of Cae A (Fig. 1A). Cae A demonstrated selective growth inhibition in TNBC cells, evidenced by lower half maximum inhibitory concentration (IC_{50}) values compared to other tumor cell lines (Fig. 1D). A significant reduction in colony numbers was observed in both 4T1 and MDA-MB-231 cells following Cae A treatment (Figs. 1B and 1C). These results indicated that Cae A exhibited specific suppressive effects on TNBC *in vitro*.

3.2. Cae A induced apoptosis in TNBC

To investigate the molecular mechanism of TNBC inhibition by Cae A, a transcriptome analysis was conducted in 4T1 cells. Cae A treatment led to 2410 up-regulated and 1174 down-regulated genes compared to untreated 4T1 cells. Differential gene enrichment analysis revealed that apoptosis signaling was among the most significantly altered pathways in 4T1 cells (Fig. 2A), indicating that Cae A might specifically trigger apoptosis in TNBC cells. Flow cytometry analysis demonstrated that 0.25 μmol·L^{-1} Cae A increased the percentage of apoptotic cells to approximately 50% after 48 h of treatment, while 0.5 μmol·L^{-1} Cae A elevated it to approximately 80% (Fig. 2B). An elevated proportion of apoptotic cells was also observed in MDA-MB-231 cells treated with Cae A (Fig. 2C). Under light microscopy, Cae A-treated 4T1 or MDA-MB-231 cells displayed inwardly contracted cell boundaries or fragmented morphology, characteristic features of apoptosis (Figs. 2D and 2E). The protein level of p-H2A.X was markedly up-regulated in TNBC cells following Cae A treatment, indicating apoptosis-associated DNA damage. Analysis of anti-apoptotic proteins Bcl-2, Bcl-xL, and pro-apoptotic protein Bax revealed significant down-regulation of Bcl-2 and Bcl-xL, along with an increased Bax/Bcl-2 ratio in Cae A-treated cells (Figs. 2F and 2G). Notably, the caspase inhibitor Z-VAD-FMK substantially suppressed Cae A-induced apoptosis (Fig. 2H) and attenuated Cae A-mediated inhibition of TNBC cells (Fig. 2I). These findings collectively demonstrated that Cae A suppressed cell growth by inducing apoptosis in TNBC cells.

3.3. Cae A induced mitochondrial dysfunction, leading to TNBC cell apoptosis

To determine whether Cae A induces apoptosis through the intrinsic pathway (mitochondrial damage pathway) or the extrinsic pathway (induced by death receptors on the cell membrane) [23], subsequent investigations focused on potential Cae A-induced mitochondrial damage. JC-1 fluorescent dye was utilized to assess mitochondrial membrane integrity. The results revealed that Cae A induced mitochondrial dysfunction, evidenced by increased green fluorescence (Fig. 3A). Examination of mitochondrial morphology using transmission electron microscopy demonstrated mitochondrial swelling and reduction or loss of mi-

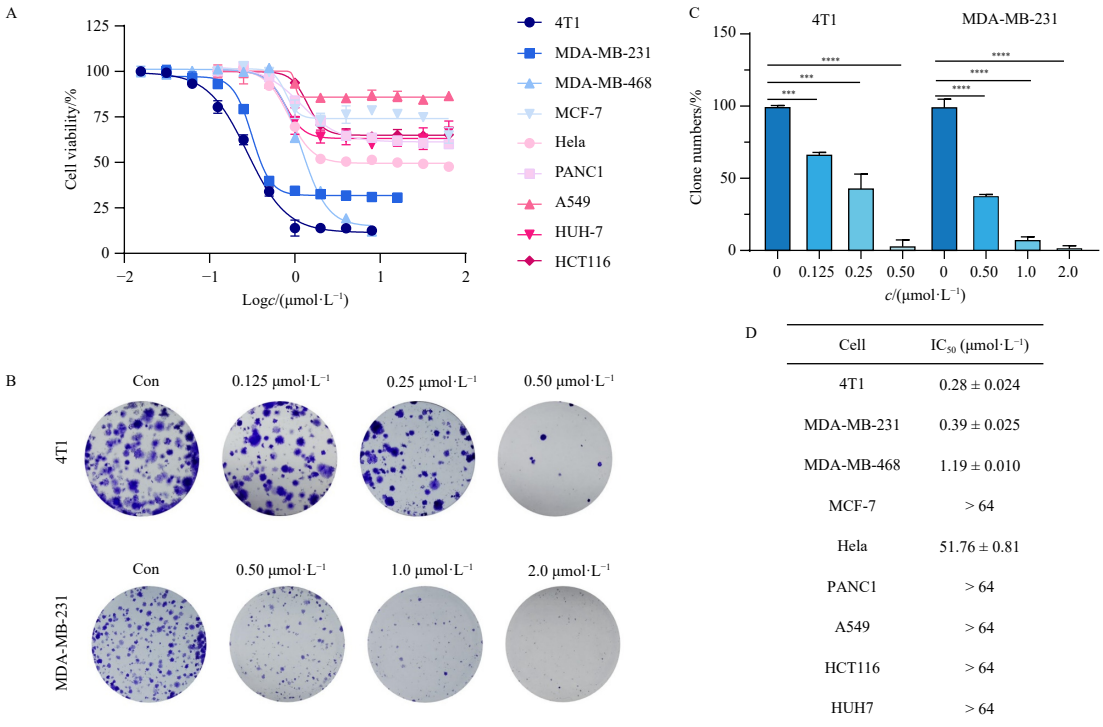

D

Cell	IC_{50} (μmol·L^{-1})
4T1	0.28 ± 0.024
MDA-MB-231	0.39 ± 0.025
MDA-MB-468	1.19 ± 0.010
MCF-7	> 64
Hela	51.76 ± 0.81
PANC1	> 64
A549	> 64
HCT116	> 64
HUH7	> 64

Fig. 1 The effect of Cae A on tumor cell proliferation and migration. (A) Cell viability of tumor cell lines treated with indicated doses of Cae A for 48 h. Cell viability was assessed by the CCK-8 assay. (B, C) Colony formation of TNBC cells after 48 h of treatment with the indicated doses of Cae A. (Scale bars = 1000 μm). (D) The half maximum inhibitory concentration (IC_{50}) of tumor cell lines treated with Cae A for 48 h. Data are presented as mean ± SD ($n = 3$). $^{***}P < 0.001$, $^{****}P < 0.0001$.

tochondrial cristae in both 4T1 cells and MDA-MB-231 cells, indicating significant Cae A-induced mitochondrial damage in TNBC cells (Fig. 3B). Analysis of cytochrome C, caspase protein family, and downstream proteins showed significant up-regulation of cytoplasmic cytochrome C, cleaved-Caspase-9, cleaved-Caspase-3, and cleaved-PARP in TNBC cells, confirming activation of the intrinsic apoptotic pathway. The expression levels of Caspase-8 proteins and cleaved-Casepase-8 protein remained unchanged, excluding involvement of the extrinsic apoptotic pathway (Figs. 3C–3E and Supplement Fig. 1). These findings demonstrated that Cae A treatment induced mitochondrial outer membrane permeabilization, leading to cytochrome C release from the mito-

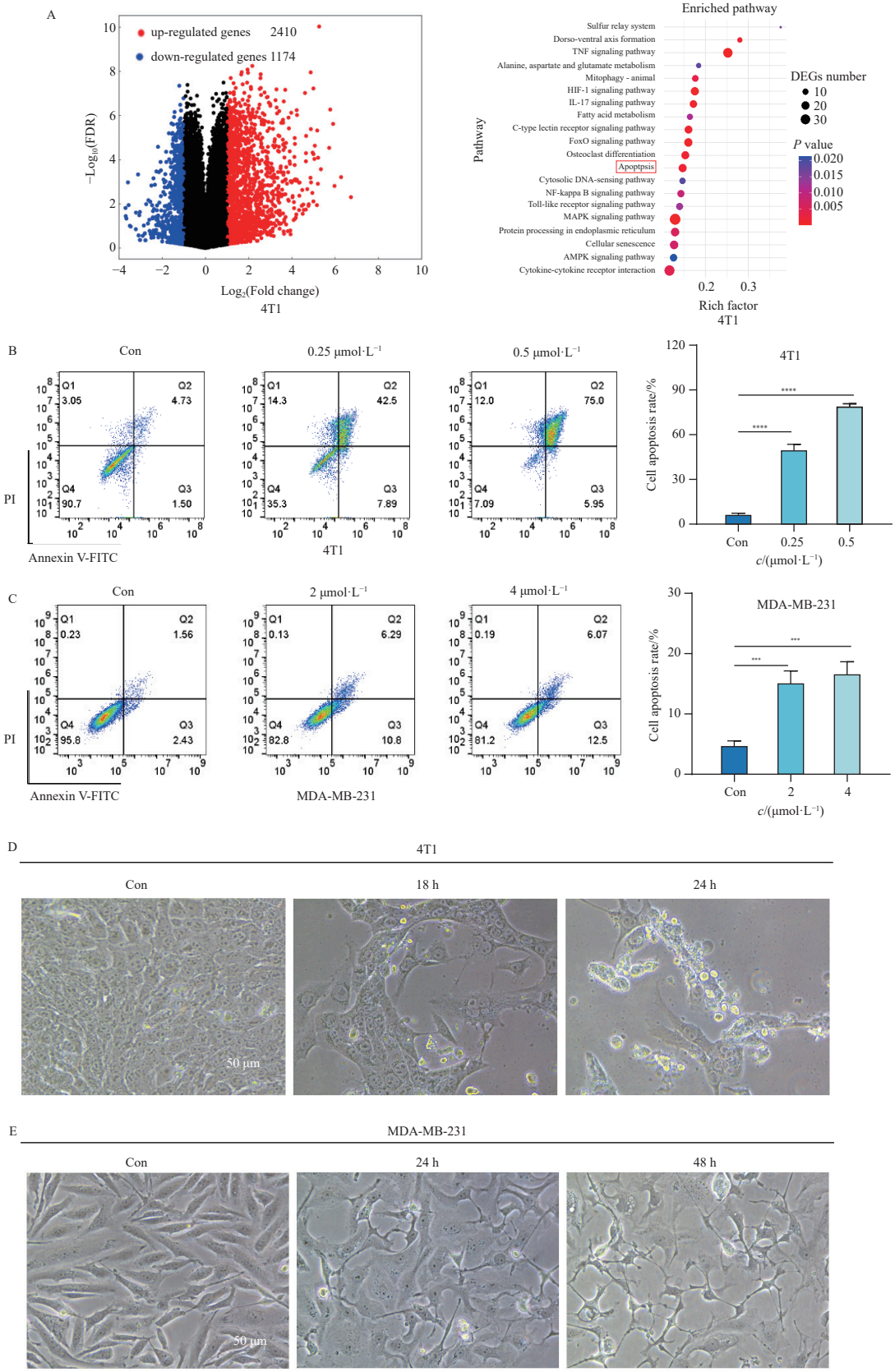

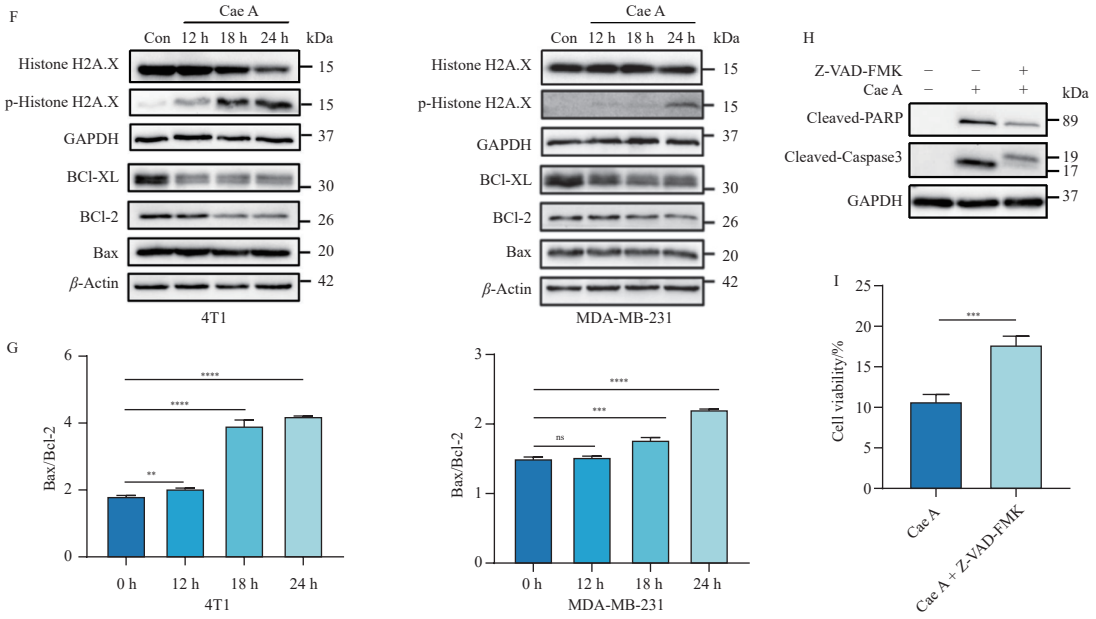

Fig. 2 Effect of Cae A on TNBC apoptosis. 4T1 cells were respectively treated with 1 μmol·L^{-1} Cae A for 12 h, and then the cells were collected for RNA sequencing. (A) Volcano map analysis of differential gene expression in 4T1 cells and the top 20 KEGG pathways for differential gene expression enrichment. (B, C) Apoptosis in Cae A-treated 4T1 and MDA-MB-231 cells. (D, E) Effect of Cae A on the morphology of 4T1 and MDA-MB-231 cells. (Scale bars = 50 μm). (F, G) The expression of p-Histone H2A.X, Bcl-xL, Bcl-2, and Bax in 4T1 and MDA-MB-231 cells. (H) Expression of cleaved-PARP and cleaved-Caspase3 in cells after treatment of 4T1 cells with 1 μmol·L^{-1} Cae A for 18 h in the presence or absence of 100 mmol·L^{-1} Z-VAD-FMK. (I) 4T1 cell growth was assessed by the CCK-8 assay. Data are presented as mean ± SD (n = 3). ns, no significance; $^{**}P$ < 0.01; $^{***}P$ < 0.001; $^{****}P$ < 0.0001.

chondrial intermembrane space and subsequent cell death.

3.4. Cae A induced sustained ER stress, leading to mitochondrial damage and intrinsic cell apoptosis in TNBC

Analysis of the top 30 genes most up-regulated by Cae A in 4T1 cells revealed that, beyond chemokines, DDIT3 (CHOP) maintained a central position in the protein interaction network (Fig. 4A). CHOP represents a target protein common to all three major ER stress sensors involved in ER stress execution. Cae A treatment significantly elevated CHOP expression in both 4T1 and MDA-MB-231 cells (Fig. 4B and 4C). Additionally, the expressions of CHOP upstream genes, including ER stress sensors *ATF6*, *p-PERK*, *p-IRE1*, and the chaperone *BiP/GRP78*, were elevated in TNBC following Cae A treatment (Figs. 4B and 4C). Previous research indicates that excessive UPR triggers apoptosis through ER stress by activating downstream ATF6, PERK, and IRE1 signaling pathways [12, 13, 24, 25]. To determine whether Cae A activated the apoptotic pathway of ER Stress in TNBC cells, we examined the expression of p-EIF2α, ATF4, and XBP1s, the downstream signaling pathways. Notably, ATF6, PERK, and IRE1 expression increased (Figs. 4B and 4C), indicating that Cae A induced irreversible and apoptosis-prone ER stress in TNBC cells. Moreover, microscopic examination revealed that Cae A-treated TNBC cells exhibited thickened ER membranes and increased vesicle numbers compared to untreated cells. The ER vesicles in TNBC cells demonstrated significant enlargement, forming distinct dilated regions. These observations further validated the aforementioned results (Fig. 3C).

The investigation suggested that mitochondrial damage induced by Cae A in TNBC cells resulted from sustained ER stress and elevated CHOP expression. To validate this hypothesis, Cae A-induced ER stress was inhibited through pre-treatment with the ER stress inhibitor 4-Phenylbutyric acid (4-PBA). The results revealed decreased expression of cleaved-PARP, cleaved-Caspase3, and Bax/Bcl-2 (Figs. 4D and 4F). Additionally, CHOP inhibition through RNA interference significantly reduced Cae A-induced cell apoptosis, accompanied by decreased levels of cleaved-PARP, cleaved-Caspase3, and Bax/Bcl-2 ratio (Figs. 4E and 4F). The suppression of CHOP expression mitigated mitochondrial membrane damage (Fig. 4G). Previous research has established ERO1A as a downstream protein of CHOP capable of inducing mitochondrial damage [26, 27]. Furthermore, reduced Bcl-2 increased mitochondrial membrane permeability [28, 29]. In 4T1 cells, CHOP protein knockdown using small interfering RNA (siRNA) counteracted both Cae A-induced *ero1a* up-regulation and Bcl-2 reduction (Supplement Fig. 2 and Fig. 4E). These findings collectively demonstrated that Cae A-induced mitochondrial dysfunction and apoptosis in TNBC cells primarily depended on CHOP up-regulation promoted by persistent ER stress.

3.5. Cae A induced abnormal glucose metabolism and triggered ER stress in TNBC Cells

Analysis of transcriptome data from 4T1 cells treated with Cae A revealed significant activation of ER stress-related signaling pathways compared to control conditions (Figs. 5A and 5B). The *DDIT3* gene, downstream of the ER stress pathway, showed particularly notable up-regulation, consistent with previous Western blotting results (Fig. 4B). The data also indicated down-regulation of tricarboxylic acid cycle-related genes, *idh1* and *ogdh*, suggesting impaired cellular oxidative phosphorylation and subsequent insufficient ATP production (Fig. 5C). Additional analysis revealed that 4T1 cells were unable to effectively increase glycolysis-related gene expression (including *aldoa*, *eno2*, *pgk1*) to compensate for energy deficiency (Fig. 5D). This limitation potentially stemmed from the low baseline levels of glycolysis genes in 4T1 cells, resulting in insufficient glycolytic reserve capacity. These observations suggested that Cae A-induced glucose metabolism disorder in the ER might serve as a direct or indirect trigger for the ER stress response in 4T1 cells.

To examine Cae A's impact on cellular energy metabolism, OCR and ECAR measurements were conducted to assess mitochondrial function and glycolysis. Cae A treatment significantly reduced OCR across all breast cancer cell lines, evidenced by decreased basal respiration and maximal respiratory capacity, indicating impaired mitochondrial oxidative phosphorylation (Figs. 5E and 5F). Additionally, Cae A treatment substantially de-

creased glycolytic reserve capacity in TNBC cells (Figs. 5E and 5G). These findings demonstrated that Cae A treatment compromised both mitochondrial oxidative phosphorylation and glycolytic metabolism in TNBC cells, thereby promoting apoptosis.

3.6. Cae A exhibited anti-cancer effect against TNBC in the murine model and organoids

As demonstrated in Figs. 6A–6D, Cae A-treated mice exhib-

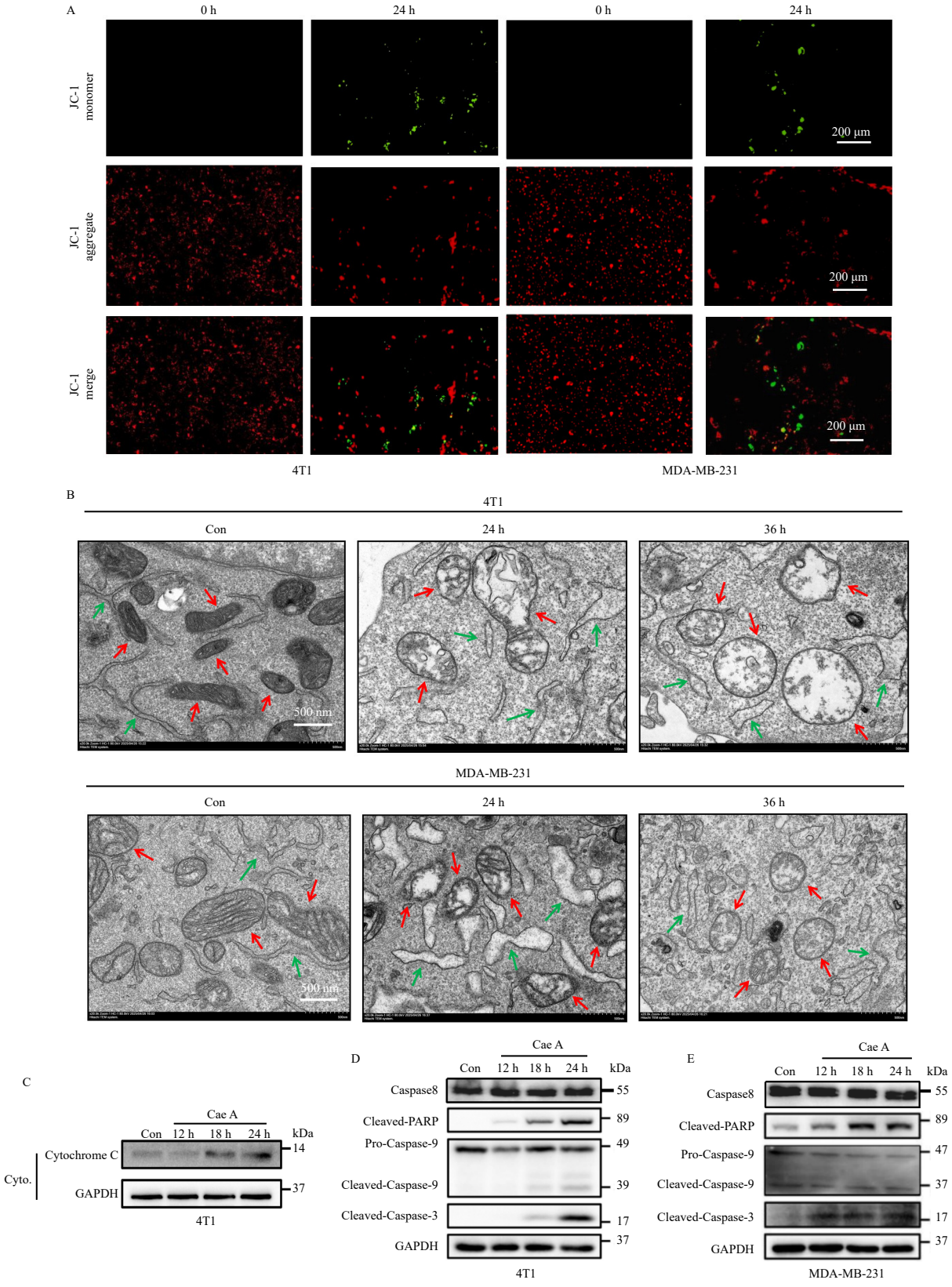

Fig. 3 The effect of Cae A on mitochondria in TNBC cells. (A) 4T1 and MDA-MB-231 cells were treated with Cae A for 24 h, then the mitochondrial membrane was stained with JC-1 dye. (Scale bars = 200 μm). (B) Electron microscopy images of mitochondria after treatment of 4T1 cells with 1 μmol·L^{-1} Cae A and MDA-MB-231 cells with 4 μmol·L^{-1} Cae A for a certain period of time (red: mitochondria; green: endoplasmic reticulum). (Scale bars = 500 nm). (C) The expression of cytosolic cytochrome C in 4T1 cytoplasm. (D, E) The expressions of Caspase-9, cleaved-Casepase-3, and cleaved-PARP in 4T1 and MDA-MB-231 cells.

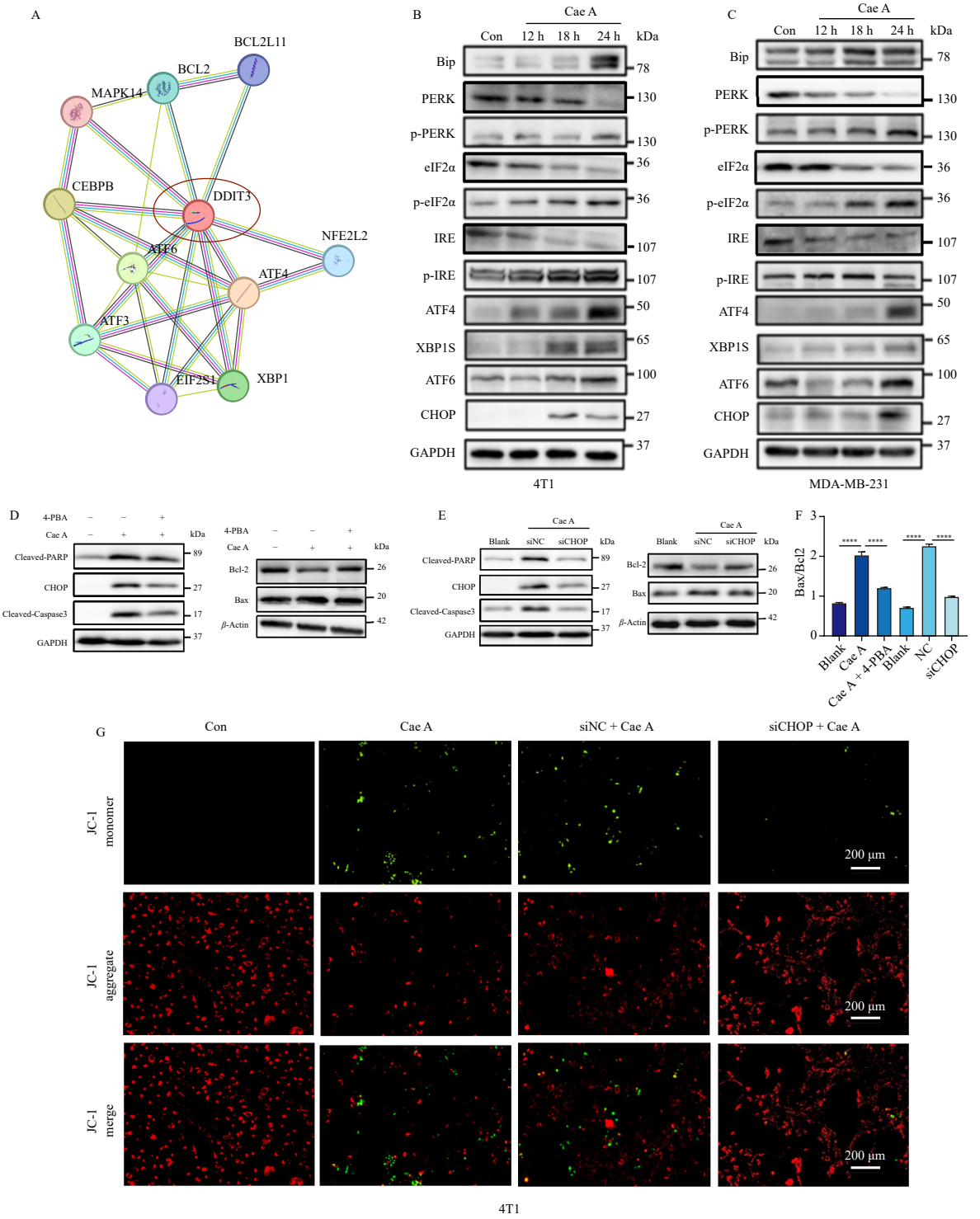

Fig. 4 The effect of Cae A on ER stress and its downstream mitochondrial damage. (A) The top 30 up-regulated genes were subjected to STRING network interaction analysis. 4T1 cells were treated with 1 μmol·L−1 Cae A and MDA-MB-231 cells were treated with 4 μmol·L−1 Cae A. Cells were collected for Western blotting 12, 18, and 24 h later. (B, C) The expression of CHOP, Bip, p-PERK, ATF4, p-eIF2α, p-IRE, XBP1S and ATF6 in cells treated with Cae A. (D) 4T1 cells were treated with 1 μmol·L^{-1} Cae A in the presence of 2 mmol·L^{-1} 4-PBA for 18 h; the expressions of CHOP, cleaved-Caspase-3, cleaved-PARP, Bax and Bcl-2 were assessed by the Western blotting assay. (E) 4T1 cells were transfected with CHOP siRNA (siCHOP) for 24 h, followed by treatment with 1 μmol·L^{-1} Cae A for 18 h, the expression of CHOP, cleaved-Caspase-3, cleaved-PARP, Bax, and Bcl-2 was assessed by western blotting. (F) Quantification of Bax/Bcl-2 Protein Expression. (G) 4T1 cells were transfected with 50 nmol·L^{-1} siNC or siCHOP for 24 h, followed by treatment with 1 μmol·L^{-1} Cae A for another 24 h, and the changes in mitochondrial membrane permeability (ΔΨ) were assessed by JC-1 staining. (Scale bars = 200 μm). $^{****}P < 0.000\,1$.

ited a significant reduction in the size, weight, and growth rate of TNBC xenografts compared with the vehicle and NC group. Terminal deoxynucleotidyl transferase-mediated dUTP nick end labeling (TUNEL) staining revealed that the tumor necrosis area in the Cae A group was substantially higher than in the vehicle and NC groups. Additionally, Cae A treatment resulted in decreased MKI67/Ki-67 staining compared with the controls, while demonstrating enhanced CHOP and cleaved-Caspase3 expression (Figs. 6E and 6F). The results of *in vivo* 4T1 transplantation tumor experiments in mice corroborated the previous *in vitro* findings. Cae A treatment significantly elevated the expression of CHOP protein, an ER stress marker, which subsequently enhanced cleaved-Caspase3 activation, promoting apoptosis. Immunofluorescence and immunohistochemistry experiments confirmed increased ap-

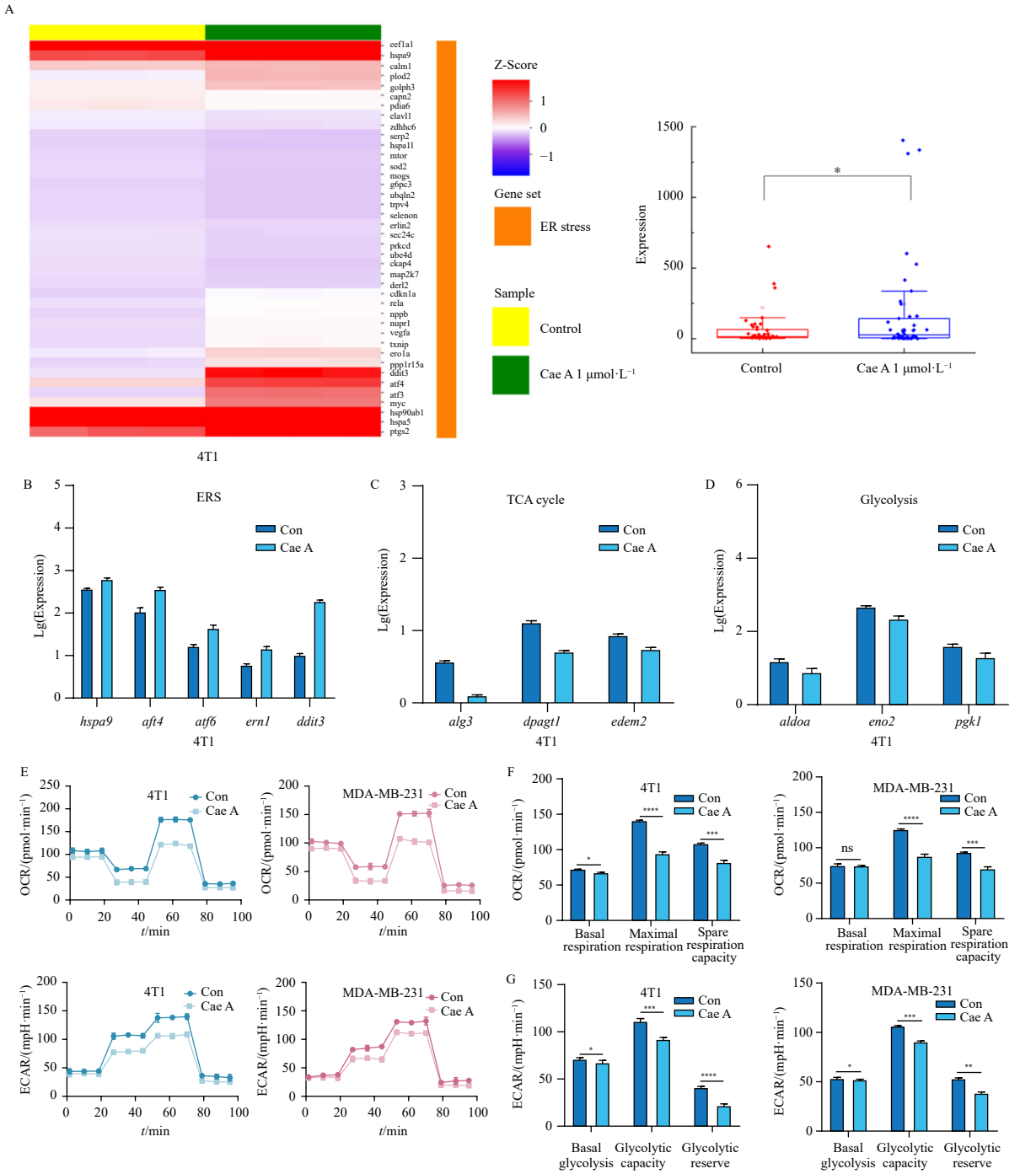

Fig. 5 Effect of Cae A on glucose metabolism and the ER. (A) Analysis of transcriptome data related to ER stress pathway in 4T1 cells. (B–D) Changes in the expression levels of ER stress, TCA cycle, and glycolysis genes in 4T1 cells. (E–G) Effect of Cae A on OCR and ECAR in TNBC cells. ns, no significance; *P < 0.05; **P < 0.01; ***P < 0.001; ****P < 0.000 1.

optosis and reduced Ki67 expression in Cae A-treated tumor cells (Fig. 6G). Notably, blood biochemical biomarker analysis indicated that Cae A exhibited no significant toxicity to liver and kidney function in mice (Fig. 6H). Furthermore, Cae A treatment showed no notable effect on the mouse body weight and organs (Figs. 6I–6K). In the evaluation of Cae A's effect on human TNBC and breast cancer organoids, Figs. 6L and 6M demonstrated that Cae A exhibited greater efficacy in inhibiting TNBC organoid proliferation compared to epirubicin and gemcitabine. The IC_{50} values for TNBC organoid inhibition were 3.13, 3.45, and 22.56 μmol·L^{-1} for Cae A, epirubicin, and gemcitabine, respectively, indicating Cae A's superior inhibitory effects against TNBC. Collectively, these findings demonstrated that Cae A exhibited potent anti-TNBC effects in mice models and organoids with minimal adverse effects.

4. Discussion

TNBC presents substantial clinical challenges due to its aggressive nature, absence of targeted therapies, elevated recurrence rates, and resistance to conventional treatments [30]. This investigation demonstrated that Cae A effectively inhibited TNBC cells, potentially through disrupting energy metabolism balance and triggering the ER stress mechanism, ultimately inducing cell apoptosis. The findings revealed that Cae A exhibited selective inhibitory effects on various cancer cell lines, with TNBC cells demonstrating heightened sensitivity, as evidenced by notably lower IC_{50} values compared to other tumor cell types. Cae A

demonstrated significant anti-tumor activity in TNBC xenograft models without apparent side effects. Furthermore, Cae A exhibited substantial inhibitory effects on TNBC organoid proliferation. These findings suggest that Cae A may represent a promising candidate as a targeted therapeutic agent for TNBC.

Transcriptomic analysis revealed that apoptotic signaling represented one of the most significantly altered pathways in Cae A-treated 4T1 cells. Flow cytometry results confirmed that Cae A substantially increased the proportion of apoptotic cells in a dose-dependent manner. The elevated p-H2A.X level indicated that Cae A treatment induced apoptosis-associated DNA damage. Notably, the study demonstrated that Cae A primarily triggered apoptosis through the intrinsic (mitochondrial) pathway. JC-1 staining results showed a significant increase in mitochondrial membrane depolarization following Cae A treatment, indicating mitochondrial dysfunction. This observation was corroborated by the increased expression of key apoptosis-related proteins, including cytosolic cytochrome C, cleaved-Caspase-9, cleaved-Caspase-3, and cleaved-PARP, which are characteristic markers of mitochondrial-mediated apoptosis. Mitochondrial-mediated apoptosis in tumors not only induces cell death but also serves a crucial function in activating immune responses, particularly through cluster of differentiation 8 $(CD8)^+$ T cell-mediated killing and the establishment of immune memory [31]. During apoptosis, the release of damage-associated molecular patterns (DAMPs), such as cytochrome c, ATP, HMGB1, and calreticulin, facilitates the recruit-

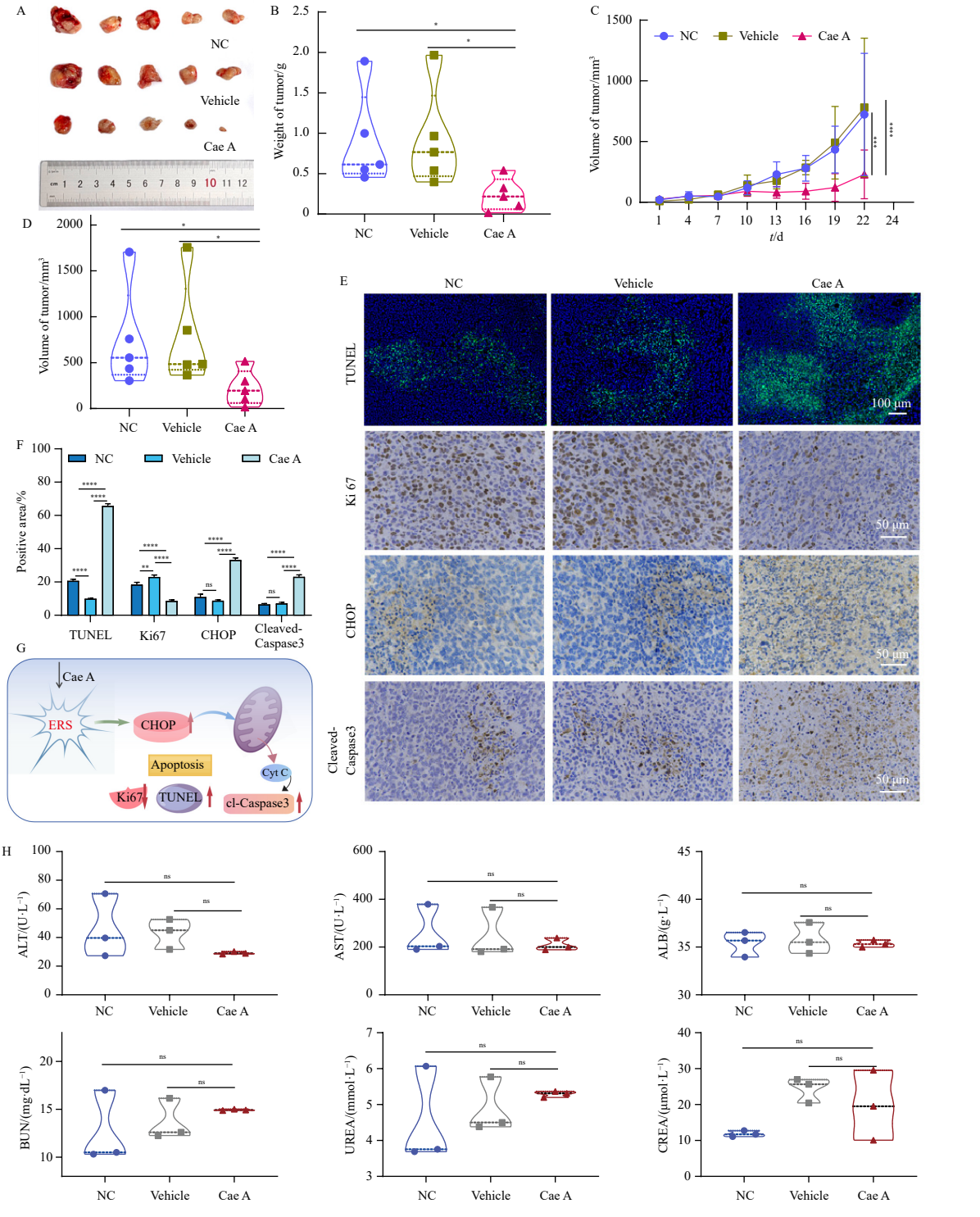

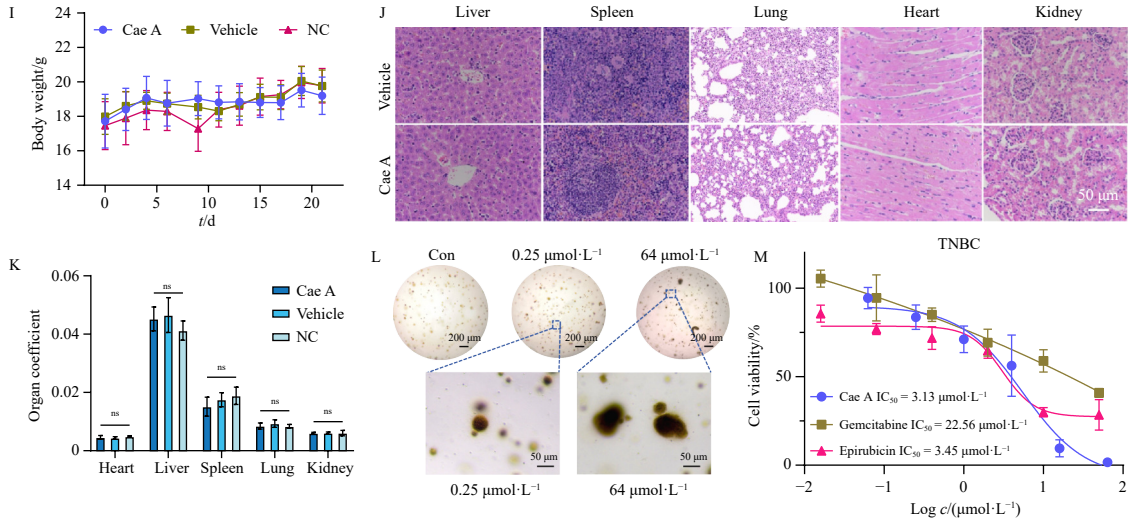

Fig. 6 Effect of Cae A on TNBC tumor growth *in vivo*. (A–D) Tumor xenograft data: representative tumor images (A), tumor weights (B) (n = 5), growth curves (C), and tumor volumes (D) in treated and control groups (n = 5). (E) TUNEL staining and IHC staining of Ki-67, CHOP and cleaved-Caspase-3 in tumor tissues (Scale bars = 100 μm/50 μm). (F) Quantitative analysis of TUNEL and IHC staining results (n = 3). (G) Schematic illustration of the proposed mechanism by which Cae A exerts tumor-suppressive effects *in vivo*. (H) Serum biochemical parameters (ALT, AST, ALB, BUN, UREA, and CREA) measured in treated mice. (n = 3). (I) Body weight curves of mice during treatment. (J) H&E staining of major organs (heart, liver, spleen, lung, and kidney) (n = 3). (Scale bars = 50 μm). (K) Organ coefficients for each group (n = 6). (L) Representative bright-field images of patient-derived TNBC organoids after 6 days of treatment with Cae A. High concentrations inhibited organoid growth. (Scale bars = 200/50 μm). (M) Organoid viability after 6 days of treatment with varying concentrations of Cae A, gemcitabine, or epirubicin, measured using the CellTiter-Glo® Luminescent Cell Viability Assay (n = 4). ns,no significance; $^{*}P < 0.05$; $^{**}P < 0.01$; $^{***}P < 0.001$; $^{****}P < 0.000\ 1$.

ment and activation of dendritic cells, which subsequently cross-prime $CD8^+$ T cells. These activated $CD8^+$ T cells target tumor cells presenting identical antigens, enhancing tumor cell elimination. Additionally, the activation of memory $CD8^+$ T cells suggests that mitochondrial-mediated apoptosis may contribute to long-term immune surveillance, potentially preventing tumor recurrence. This immune response can be enhanced by immune checkpoint inhibitors, which augment $CD8^+$ T cell activity by blocking inhibitory pathways such as PD-1/PD-L1 [32]. Thus, the apoptosis induced by Cae A could initiate the host's anti-tumor immune responses, establishing its potential as an anti-tumor drug for combination with immune checkpoint inhibitors.

ER as a central organelle in eukaryotic cells, plays a crucial role in various synthetic processes, including protein synthesis, modification, and lipid production [10, 33]. Due to rapid proliferation and robust metabolism, tumor cells typically require increased protein synthesis compared to normal cells, making ER stress a distinctive characteristic of cancer cells [34, 35]. Consequently, cytotoxic compounds targeting the ER demonstrate greater selectivity towards cancer cells than non-cancer cells [13]. Researchers have proposed two approaches to target the ER based on different types of ER stress: either inhibiting the UPR to reduce ER stress levels, thereby increasing the accumulation of unfolded and misfolded proteins and heightening cellular stress to induce cell death, for example, by silencing the expression of BiP, IRE, XBP1, and PERK, or using corresponding inhibitors [36-38]; or enhancing ER stress levels to induce apoptosis [39, 40], such as by up-regulating the expression of CHOP, a key protein in this process [41, 42]. Currently, anti-tumor agents like Velcade (Bortezomib), a highly selective proteasome inhibitor approved for treating malignant tumors either alone or in combination with chemotherapy, promote apoptosis by inducing excessive ER stress [43, 44]. The findings indicated that CHOP level was significantly elevated in TNBC cells after Cae A treatment, accompanied by increased levels of upstream ER stress sensors such as ATF6, p-PERK and p-IRE1. Blocking ER stress with the inhibitor 4-PBA or silencing CHOP expression substantially reduced Cae A-induced apoptosis and mitochondrial damage, confirming the essential role of ER stress in Cae A-mediated cell death. As an inhibitor of ER stress, 4-PBA reduced the expression of CHOP induced by Cae A in TNBC. Analysis of potential downstream target genes of CHOP revealed that after Cae A-induced mitochondrial stress in TNBC cells, the level of *ero1a* downstream of CHOP significantly increased, while Bcl-2 levels decreased. Up-regulation of CHOP protein following intracellular ER stress can induce ero1a up-regulation which is involved in mitochondrial damage [26, 27]. When *ero1a* was knocked down, mitochondrial damage was reduced. Previous research indicates that a decrease in Bcl-2 can result in increased mitochondrial membrane permeability [7, 8]. When CHOP levels were reduced using siRNA, *ero1a* levels decreased, and Bcl-2 levels increased. These findings suggest that the over-expressed CHOP induces mitochondrial damage by up-regulating *ero1a* and down-regulating Bcl-2.

Previous research has demonstrated that metabolic abnormalities can disrupt ER homeostasis, leading to ER stress and UPR activation [45, 46]. Through transcriptomic data analysis, this study investigated the relationship between Cae A-induced ER stress and glucose metabolism disruption. In 4T1 cells treated with 1 $\mu mol \cdot L^{-1}$ of Cae A, genes associated with the tricarboxylic acid cycle exhibited significant downregulation, while glycolysis reserve capacity proved insufficient, resulting in inadequate cellular energy supply. These factors were identified as potential triggers of ER stress and cell apoptosis. The seahorse assay validated these hypotheses, demonstrating that Cae A substantially inhibited the OCR and ECAR of TNBC cells, thereby reducing mitochondrial respiration and glycolysis. This suggests that TNBC cells experienced energy metabolism deprivation and struggled to meet their energy requirements. The energy metabolism imbalance showed a strong correlation with ER stress. Energy metabolism dysregulation reduced ATP synthesis, impacting ATP-dependent molecular chaperons (such as BiP) in the ER, resulting in unfolded protein accumulation and UPR activation. Thus, energy deficiency likely induced ER stress in Cae A-treated TNBCs.

Breast cancer organoids serve as an effective model for evaluating anti-tumor drug efficacy. Cae A demonstrated comparable effectiveness to epirubicin in TNBC organoids (IC_{50}: 3.13 $\mu mol \cdot L^{-1}$ *vs* 3.45 $\mu mol \cdot L^{-1}$), while showing significantly greater potency than gemcitabine (IC_{50}: 3.13 $\mu mol \cdot L^{-1}$ *vs* 22.56 $\mu mol \cdot L^{-1}$). These results indicate Cae A's potential for clinical application. Given TNBC's aggressive nature and limited response to conventional therapies, the identification of effective treatments like Cae A holds particular significance. Pending confirmation through addi-

tional preclinical and clinical studies regarding safety and efficacy, Cae A may provide a valuable alternative or complementary approach to existing TNBC treatments, potentially enhancing patient outcomes through resistance mitigation and improved treatment effectiveness.

In conclusion, this study established that Cae A inhibited TNBC cell growth through modulation of glucose metabolism disorders and induction of a sustained ER stress/mitochondrial dysfunction/apoptosis signaling pathway. The specific ER stress induction triggered by abnormal glucose metabolism underscores Cae A's potential as an effective therapeutic agent for TNBC. Future research should address the targeted delivery of Cae A and investigate its clinical applications in TNBC treatment.

Funding

This work was supported by the Science and Education Integration Project by the Innovation and Entrepreneurship Office of Nanjing University (No. 0214-1480608207) and Jiangsu Provincial Research Hospital (No. YJXYY202204).

Declaration of competing interest

These authors have no conflict of interest to declare.

References

1 Siegel RL, Miller KD, Wagle NS, et al. Cancer statistics, 2023. *CA: A Cancer J Clin*. 2023;73(1):17-48. https://doi.org/10.3322/caac.21763.
2 Goldhirsch A, Winer EP, Coates AS, et al. Personalizing the treatment of women with early breast cancer: highlights of the St Gallen International Expert Consensus on the Primary Therapy of Early Breast Cancer 2013. *Ann Oncol*. 2013;24(9):2206-2223. https://doi.org/10.1093/annonc/mdt303.
3 Jiang YZ, Ma D, Suo C, et al. Genomic and transcriptomic landscape of triple-negative breast cancers: subtypes and treatment strategies. *Cancer Cell*. 2019;35(3):428-440. e5. https://doi.org/10.1016/j.ccell.2019.02.001.
4 Cancer Genome Atlas Network. Comprehensive molecular portraits of human breast tumours. *Nature*. 2012;490(7418): 61-70. https://doi.org/10.1038/nature11412.
5 Ganesan P, Moulder S, Lee JJ, et al. Triple-negative breast cancer patients treated at MD Anderson Cancer Center in phase I trials: improved outcomes with combination chemotherapy and targeted agents. *Mol Cancer Therapeut*. 2014;13(12):3175-3184.https://doi.org/10.1158/1535-7163.MCT-14-0358.
6 Lyons TG. Targeted therapies for triple-negative breast cancer. *Curr Treat Options Oncol*. 2019;20(11):82. https://doi.org/10.1007/s11864-019-0682-x.
7 Sasaki K, Yoshida H. Organelle autoregulation-stress responses in the ER, Golgi, mitochondria and lysosome. *J Biochem*. 2015;157(4):185-195. https://doi.org/10.1093/jb/mvv010.
8 Luo B, Lee AS. The critical roles of endoplasmic reticulum chaperones and unfolded protein response in tumorigenesis and anticancer therapies. *Oncogene*. 2012;32(7):805-818. https://doi.org/10.1038/onc.2012.130.
9 Wang M, Kaufman RJ. The impact of the endoplasmic reticulum protein-folding environment on cancer development. *Nature Rev Cancer*. 2014;14(9):581-597. https://doi.org/10.1038/nrc3800.
10 Schröder M, Kaufman RJ. The mammalian unfolded protein response. *Ann Rev Biochem*. 2005;74(1):739-789. https://doi.org/10.1146/annurev.biochem.73.011303.074134.
11 Maurel M, McGrath EP, Mnich K, et al. Controlling the unfolded protein response-mediated life and death decisions in cancer. *Semin Cancer Biol*. 2015;33:57-66. https://doi.org/10.1016/j.semcancer.2015.03.003.
12 Ferri KF, Kroemer G. Organelle-specific initiation of cell death pathways. *Nat Cell Biol*. 2001;3(11):E255-263. https://doi.org/10.1038/ncb1101-e255.
13 King AP, Wilson JJ. Endoplasmic reticulum stress: an arising target for metal-based anticancer agents. *Chem Soc Rev*. 2020;49(22):8113-8136. https://doi.org/10.1039/D0CS00259C.
14 Kim C, Kim B. Anti-cancer natural products and their bioactive compounds inducing ER stress-mediated apoptosis: a review. *Nutrients*. 2018;10(8):1021. https://doi.org/10.3390/nu10081021.
15 Liu S, Zhang X, Yao X, et al. Mammalian IRE1α dynamically and functionally coalesces with stress granules. *Nat Cell Biol*. 2024;26(6):917-931. https://doi.org/10.1038/s41556-024-01418-7.
16 Wang HF, Wang ZQ, Ding Y, et al. Endoplasmic reticulum stress regulates oxygen-glucose deprivation-induced parthanatos in human SH-SY5Y cells *via* improvement of intracellular ROS. *CNS Neurosci Ther*. 2018;24(1):29-38. https://doi.org/10.1111/cns.12771.
17 Geng H, Chen L, Lv S, et al. Photochemically controlled release of the glucose transporter 1 inhibitor for glucose deprivation responses and cancer suppression research. *J Proteome Res*. 2024;23(2):653-662. https://doi.org/10.1021/acs.jproteome.3c00469.
18 Wu L, Jin Y, Zhao X, et al. Tumor aerobic glycolysis confers immune evasion through modulating sensitivity to T cell-mediated bystander killing *via* TNF-α. *Cell Metab*. 2023;35(9):1580-1596. e9. https://doi.org/10.1016/j.cmet.2023.07.001.
19 Bérdy J. Bioactive microbial metabolites. *J Antibiot (Tokyo)*. 2005;58(1):1-26. https://doi.org/10.1038/ja.2005.1.
20 Funk A, Divekar PV. Caerulomycin, a new antibiotic from *Streptomyces caeruleus* Baldacci. I. Production, isolation, assay, and biological properties. *Can J Microbiol*. 1959;5:317-321. https://doi.org/10.1139/m59-039.
21 Balachandran C, Hirose M, Tanaka T, et al. Design and synthesis of poly(2,2′-bipyridyl) ligands for induction of cell death in cancer cells: control of anticancer activity by complexation/decomplexation with biorelevant metal cations. *Inorganic Chem*. 2023;62(36):14615-14631. https://doi.org/10.1021/acs.inorgchem.3c01738.
22 Mitchell RJ, Gowda AS, Olivelli AG, et al. Triarylphosphine-coordinated bipyridyl Ru(II) complexes induce mitochondrial dysfunction. *Inorganic Chem*. 2023;62(28):10940-10954. https://doi.org/10.1021/acs.inorgchem.3c00736.
23 Carneiro BA, El-Deiry WS. Targeting apoptosis in cancer therapy. *Nat Rev Clin Oncol*. 2020;17(7):395-417. https://doi.org/10.1038/s41571-020-0341-y.
24 Verfaillie T, Garg AD, Agostinis P. Targeting ER stress induced apoptosis and inflammation in cancer. *Cancer Lett*. 2013;332(2):249-264. https://doi.org/10.1016/j.canlet.2010.07.016.
25 Bock FJ, Tait SWG. Mitochondria as multifaceted regulators of cell death. *Nat Rev Mol Cell Biol*. 2020;21(2):85-100. https://doi.org/10.1038/s41580-019-0173-8.
26 Li G, Mongillo M, Chin KT, et al. Role of ERO1-α-mediated stimulation of inositol 1,4,5-triphosphate receptor activity in endoplasmic reticulum stress-induced apoptosis. *J Cell Biol*. 2009;186(6):783-792. https://doi.org/10.1083/jcb.200904060.
27 Lai L, Liu Y, Liu Y, et al. Role of endoplasmic reticulum oxidase 1α in H9C2 cardiomyocytes following hypoxia/reoxygenation injury. *Mol Med Rep*. 2020;22(2):1420-1428. https://doi.org/10.3892/mmr.2020.11217.
28 Wang LL, Hu RC, Dai AG, et al. CHOP overexpression sensitizes human non-small cell lung cancer cells to cisplatin treatment by Bcl-2/JNK pathway. *Am J Transl Res*. 2021;13(6):6279-6287.
29 Li Y, Jiang W, Niu Q, et al. eIF2α-CHOP-BCl-2/JNK and IRE1α-XBP1/JNK signaling promote apoptosis and inflammation and support the proliferation of Newcastle disease virus. *Cell Death Dis*. 2019;10(12):891. https://doi.org/10.1038/s41419-019-2128-6.
30 Waks AG, Winer EP. Breast cancer treatment: a review. *JAMA*. 2019;321(3):288-300. https://doi.org/10.1001/jama.2018.19323.
31 Kroemer G, Galluzzi L, Kepp O, et al. Immunogenic cell death in cancer therapy. *Annu Rev Immunol*. 2013;31:51-72. https://doi.org/10.1146/annurev-immunol-032712-100008.
32 Sprooten J, Laureano RS, Vanmeerbeek I, et al. Trial watch: chemotherapy-induced immunogenic cell death in oncology. *Oncoimmunology*. 2023;12(1):2219591. https://doi.org/10.1080/2162402X.2023.2219591.
33 Kaufman RJ. Orchestrating the unfolded protein response in health and disease. *J Clin Invest*. 2002;110(10):1389-1398. https://doi.org/10.1172/JCI0216886.
34 Walczak A, Gradzik K, Kabzinski J, et al. The role of the ER-induced UPR pathway and the efficacy of its inhibitors and inducers in the inhibition of tumor progression. *Oxid Med Cell Longev*. 2019;2019:5729710. https://doi.org/10.1155/2019/5729710.
35 Urra H, Dufey E, Lisbona F, et al. When ER stress reaches a dead end. *Biochim Biophys Acta*. 2013;1833(12):3507-3517. https://doi.org/10.1016/j.bbamcr.2013.07.024.
36 Rangel DF, Dubeau L, Park R, et al. Endoplasmic reticulum chaperone GRP78/BiP is critical for mutant Kras-driven lung tumorigenesis. *Oncogene*. 2021;40(20):3624-3632. https://doi.org/10.1038/s41388-021-01791-9.
37 Liu Y, Adachi M, Zhao S, et al. Preventing oxidative stress: a new role for XBP1. *Cell Death Differ*. 2009;16(6):847-857. https://doi.org/10.1038/cdd.2009.14.
38 Papandreou I, Denko NC, Olson M, et al. Identification of an Ire1alpha endonuclease specific inhibitor with cytotoxic activity against human multiple myeloma. *Blood*. 2011;117(4):1311-1314. https://doi.org/10.1182/blood-2010-08-303099.
39 Tabas I, Ron D. Integrating the mechanisms of apoptosis induced by endoplasmic reticulum stress. *Nat Cell Biol*. 2011;13(3):184-190. https://doi.org/10.1038/ncb0311-184.
40 Li J, Ni M, Lee B, et al. The unfolded protein response regulator GRP78/BiP is required for endoplasmic reticulum integrity and stress-induced autophagy in mammalian cells. *Cell Death Differ*. 2008;15(9):1460-1471. https://doi.org/10.1038/cdd.2008.81.
41 Huber AL, Lebeau J, Guillaumot P, et al. p58(IPK)-mediated attenuation of the proapoptotic PERK-CHOP pathway allows malignant progression upon low glucose. *Mol Cell*. 2013;49(6):1049-1059. https://doi.org/10.1016/j.molcel.2013.01.009.
42 Nakagawa H, Umemura A, Taniguchi K, et al. ER stress cooperates with hypernutrition to trigger TNF-dependent spontaneous HCC development. *Cancer Cell*. 2014;26(3):331-343. https://doi.org/10.1016/j.ccr.2014.07.001.
43 Obeng EA, Carlson LM, Gutman DM, et al. Proteasome inhibitors induce a terminal unfolded protein response in multiple myeloma cells. *Blood*. 2006;107(12):4907-4916. https://doi.org/10.1182/blood-2005-08-3531.
44 Chen B, Lei S, Yin X, et al. Mitochondrial respiration inhibition suppresses papillary thyroid carcinoma *via* PI3K/Akt/FoxO1/Cyclin D1 pathway. *Front Oncol*. 2022;12:900444. https://doi.org/10.3389/fonc.2022.900444.
45 Kunimasa K, Ikeda-Ishikawa C, Tani Y, et al. Spautin-1 inhibits mitochondrial complex I and leads to suppression of the unfolded protein response and cell survival during glucose starvation. *Sci Rep*. 2022;12(1):11533. https://doi.org/10.1038/s41598-022-15673-x.
46 Shao M, Shan B, Liu Y, et al. Hepatic IRE1α regulates fasting-induced metabolic adaptive programs through the XBP1s-PPARα axis signalling. *Nat Commun*. 2014;5:3528. https://doi.org/10.1038/ncomms4528.